Journal of Manufacturing Innovations
2024, VOL. 1, NO. 2, 28-35
DOI: 10.22055/jomi.2024.46962.1019

Microstructural Evolution of CMSX-4 Single Crystal Superalloy with Varying Distance from the Chill Plate

Ali Jadidi* , Seyyed Mehdi Abbasi , Masoume Seifollahi

Metallic Materials Research Center, Malek Ashtar University of Technology, Tehran, Iran

ABSTRACT

The microstructural characteristics of the CMSX-4 single crystal produced by the Bridgman method at a withdrawal rate of 2 mm/min, was investigated through experimental measurements as a function of the distance from chill plate in the present study. The single crystal examined in this research was fabricated using a vertical Bridgman device equipped with a radiation baffle. The microstructural characteristics of the primary dendrite arm spacing (λ_1) and the secondary dendrite arm spacing (λ_2) have been calculated from transverse and longitudinal sections at different distances from the chill plate, using software analysis of images prepared with an optical microscope (OM). The comparison of the obtained values for the microstructural characteristics λ_1 and λ_2 reveals that both variables increase with increasing distance from the chill plate by 19.6% and 18.8%, respectively, in the single crystal. Additionally, the thermal gradient has been calculated based on the primary and secondary dendrite arm spacing and the result obtained from the primary dendrite arm spacing was found to be more reasonable due to its better alignment with experimental values.

ARTICLE HISTORY
Received 23 May 2024
Revised 27 July 2024
Accepted 27 July 2024

KEYWORDS
Single crystal superalloy
Bridgman method
Chill plate
CMSX-4
Dendrite arm spacing

1. Introduction

A grain is a small or microscopic single crystal, which has a periodic arrangement of atoms. Most metals in general use are polycrystalline, thus consisting of grains separated by grain boundaries (GBs), whereas single crystal metals have a single grain throughout the entire sample and have no GBs. Single crystal metals have different properties and uses than their polycrystalline counterparts [1]. For the first time, single crystal superalloys were utilized by Pratt & Whitney Air Industries in the manufacture of engine blades and vanes in 1969. CMSX-4 is a nickel-based single-crystal superalloy that was introduced by Cannon Muskegon in 1990, and it belongs to the second generation of nickel-based single-crystal superalloys. The CMSX-4 superalloy consists of two phases, γ and γ', where γ is the matrix phase and γ' deposits are dispersed within it. The strengthening mechanism of this superalloy arises from the creation of a solid solution via the addition of Cr, W, and Ta elements, as well as the precipitation of Al and Ti elements through the formation of γ' phase [2,3].

The primary solidification parameters that have a substantial impact on the microstructure and physical properties of the final casting are the thermal gradient (G), crystal growth rate (R), and concentration of alloy elements (C_0). The evaluation of dendritic microstructure is performed based on parameters that are dependent on solidification conditions. The primary dendrite arm spacing (λ_1) is dependent on the thermal gradient, growth rate, and chemical composition. Equation 1 is a widely accepted result of most theoretical studies in this field:

$$\lambda_1 = AG^{-m}R^{-n} \qquad \text{(Eq. 1)}$$

Variables G and R represent the thermal gradient and crystal growth rate, respectively. The variable A is dependent on the chemical composition of the superalloy, whereas m and n are specific constants with values of 0.5 and 0.25, respectively. According to the research conducted by Flemings, the secondary dendrite arm spacing (λ_2) is also a function of the thermal gradient and crystal growth rate.

* Corresponding author.
E-mail address: Alijdidi13@gmail.com (A.Jadidi)

It is calculated by equation 2:

$$\lambda_2 = C(GR)^{-n} \quad \text{(Eq. 2)}$$

The variable C in equation 2 is a constant, and the value of n is 1/3 [4]. The thermal gradient in the solidification front and the crystal growth rate are two fundamental variables that play a crucial role in the formation of the microstructure of single-crystal superalloy parts [5]. According to Milenkovic and Lee's research [6], increasing the thermal gradient and crystal growth rate in M247LC nickel superalloy leads to a reduction in dendrite arm spacing, resulting in a finer microstructure. Additionally a higher thermal gradient is also found to reduce dendrite arm spacing and microsegregation. The increase in thermal gradient that occurs due to the increase in cooling rate (heat transfer rate) causes interdendritic distances to decrease, which will lead to a finer microstructure in single crystal cast parts, ultimately resulting in improved mechanical properties [7].

In Bridgman's single crystal growth process, the withdrawal rate, which is the rate of movement of the solidification front, is approximately equal to the withdrawal rate [8]. Matache et al. [9], have proposed theoretical equations 3 and 4 to calculate the primary (λ_1) and secondary (λ_2) dendritic arm spacing in CMSX-4 single crystals:

$$\lambda_1 = 255(G \cdot V)^{-0.34} \quad \text{(Eq. 3)}$$

$$\lambda_2 = 47.83(G \cdot V)^{-0.35} \quad \text{(Eq. 4)}$$

Another critical microstructural variable is the deviation of the crystal direction of the final single crystal casting from the preferred crystal orientation. In CMSX-4 single crystal castings, the preferred crystal orientation is [001], and a significant increase in deviation from this orientation leads to a substantial drop in mechanical properties at high temperatures. Additionally, the highest deviation from the preferred crystal orientation is typically observed in the upper portion of the casting, which is farthest from the chill plate. The maximum angle between the single crystal blade axis and the [001] direction should be no more than 12°, but to achieve the best mechanical properties, particularly fatigue resistance, it is desirable to maintain this angle as low as possible [10].

Based on the previous discussion, the primary objective of this research is to investigate the variations in the microstructural characteristics λ_1 and λ_2 in CMSX-4 single crystals fabricated using the vertical Bridgman method by increasing the distance from the chill plate (decreasing the thermal gradient). Additionally, this research aims to extract the thermal gradient by plotting a diagram of dendrite arm spacing versus distance from the chill plate, and then compare the experimental λ_1 and λ_2 values with theoretical results obtained from equations 3 and 4.

2. Materials and Methods

The single-crystal growth in this research was conducted in a vertical Bridgman furnace equipped with a graphite radiation baffle, utilizing the HRS method. Figure 1 presents a schematic design of this casting process. After the melt pouring operation, the mold was thermally stabilized by remaining motionless for 1 minute before being slowly moved to the cold area at a withdrawal rate of 2 mm/min. Prior to pouring, the ceramic mold was preheated to a temperature of 1500°C. The ceramic mold consists of layers of zirconia and alumina with varying particle sizes.

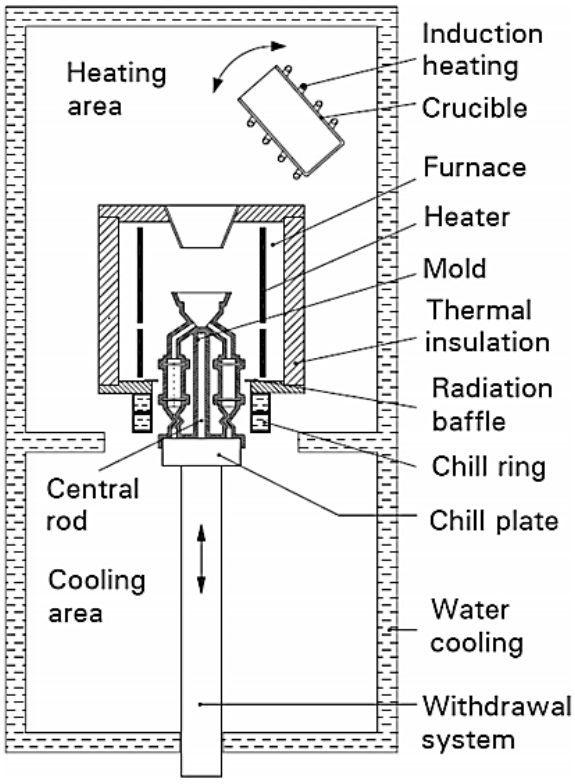

Figure 1. The schematic design of vertical Bridgman furnace [11].

Figure 2 presents a schematic image of the ceramic mold and its components. It is important to note that the described mold features a central rod for the entry of the primary melt, surrounded by four

dumbbell-shaped chambers, as depicted in the illustration.

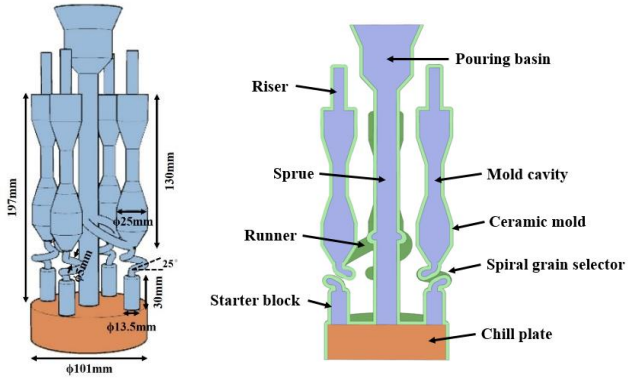

(a) (b)

Figure 2. The schematic image of (a) the ceramic mold used in the present research and (b) longitudinal cross-section of the mold.

The alloying process was performed using vacuum induction melting (VIM), and the resulting ingot was then melted in a HRS Bridgman furnace to produce single crystals. The chemical composition of the CMSX-4 superalloy ingot (Table 1) was determined using quantometry.

Table 1. The chemical composition of the CMSX-4 ingot used in the present research.

Element	Ni	Al	Ti	Cr	Co	Mo	Ta	W	Re	Hf
wt. %	Bal.	5.60	0.98	6.50	9.59	0.70	6.60	6.60	3.05	0.01

To investigate the microstructure of the final single crystal casting, cross-sections were created at specific distances from the chill plate (Figure 3). To reveal the dendrites in the obtained samples, the following etching solutions were used: Marble solution (50 ml of hydrochloric acid, 50 ml of distilled water, and 10 g of copper(II) sulfate), Kalling II solution (5 g of copper chloride, 100 ml of hydrochloric acid, and 100 ml of ethanol), and V2A solution (119 ml of hydrochloric acid, 12 ml of nitric acid, and 119 ml of distilled water). Each sample was submerged in its respective solution for 1 minute. Microstructural examination was performed using an Olympus DP 25 optical microscope.

The primary dendrite arm spacing (λ_1) was measured using the dendrite core count method in cross-sectional microstructure images analyzed with Image-J software. The number of dendrites was counted and inserted into equation 5, which was proposed by Van et al. [12]. Note that, S and N represent the areas where primary dendrites are counted and the number of primary dendrites counted, respectively. Given the regular arrangement of dendrites, the variable c in equation 5 was set equal to 1.

$$\lambda_1 = c\sqrt{\frac{S}{N}} \qquad \text{(Eq. 5)}$$

The secondary dendrite arm spacing (λ_2) was measured by calculating the distance between secondary dendrites in longitudinal cross-sectional images of the sample, obtained after etching, using Image-J software. This measurement was made according to the D method proposed by Vandersluis and Ravindran [13].

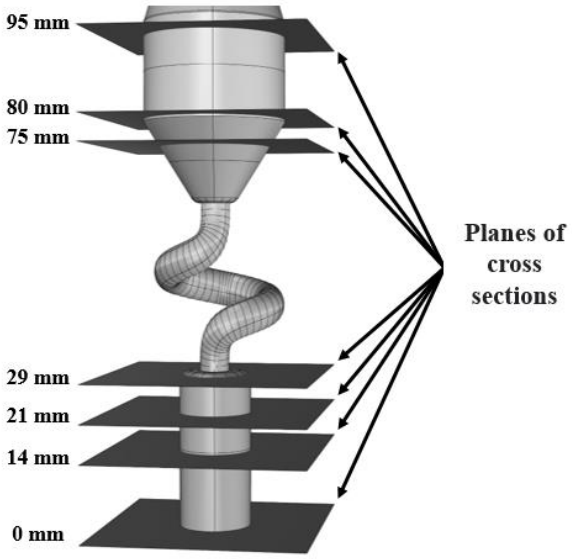

Figure 3. The schematic image of transverse cross-sections of the grain selection system and the single crystal casting.

Figure 4-a shows the single crystal casting fabricated at a withdrawal rate of 2 mm/min, featuring a grain selection system consisting of a starter block and a spiral grain selector. To verify that the final casting is single crystal, X-ray diffraction using the Laue method was performed at 9 distinct points on the cross-sectional surface, 95 mm away from the chill plate. The Laue method employed a wavelength range of 0.28 Å to 2.50 Å, and the data analysis was carried out using the OrientExpress software, as depicted in Figure 4-b. The diffraction patterns from all points showed matching results, with an angle of deviation from the preferred crystal orientation reported to be 13.5° ± 0.1°.

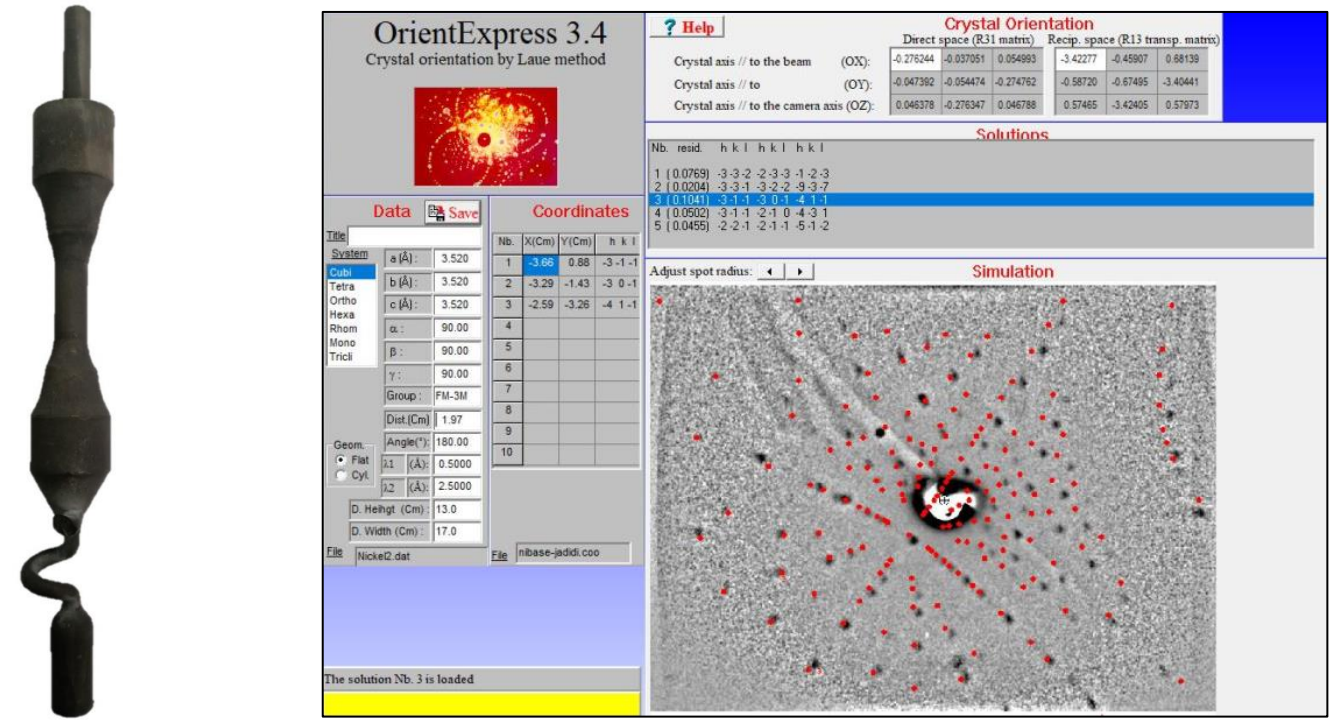

(a) (b)

Figure 4. The image of (a)dumbbell-shaped single-crystal casting with the grain selection system and (b)diffraction data analysis performed in OrientExpress software.

3. Results and Discussion

Figure 5 illustrates the microstructure of cross-sections at various distances from the chill plate in the starter block. The solidification pattern transitions from cellular (section a) to dendritic (sections b, c, and d), indicating a significant reduction in thermal gradient with increasing distance from the chill plate in this region. Section b exhibits delicate and challenging-to-distinguish dendrites, whereas sections c and d display clearly visible primary dendrites.

Figure 5. Microstructural images with 50 times magnification of cross-sections of the starter block at distances a)0, b)14, c)21 and d)29 mm from the chill plate.

According to Moreira et al. [14], the cooling rate near the chill plate is 18 °C/s, which corresponds to a G/R value greater than 16,000 °C·s/mm. Using the withdrawal rate (2 mm/min) as R and considering Lee et al.'s [15] findings, this value suggests that cellular growth is likely to occur, as presented in Figure 5-a.

The average primary dendrite arm spacing (λ_1) in sections b, c, and d of Figure 5 was calculated using equation 5, yielding values of 131, 280, and 287 micrometers, respectively. As the distance from the chill plate increases, λ_1 initially increases steeply and then levels off. The results for λ_1 in the cross-sections of Figure 5 are presented in Figure 6, with error bars included to reflect the variability.

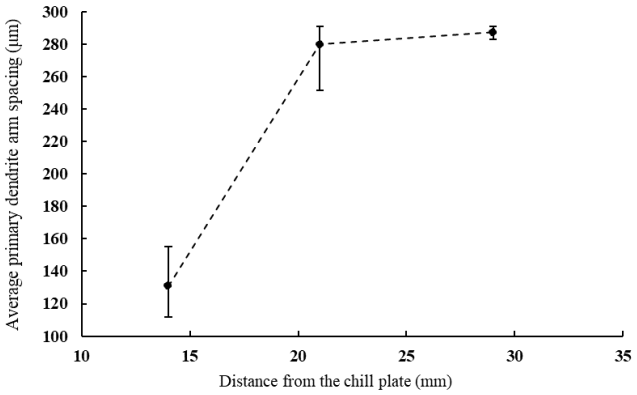

Figure 6. The diagram of the average primary dendrite arm spacing versus the distance from the chill plate (sections b, c and d of Figure 5).

As depicted in Figure 6, the slope of the increase in average primary dendrite arm spacing declines with increasing distance from the chill plate.

Notably, however, the average primary dendrite arm spacing at distances of 21 mm and 29 mm from the chill plate does not exhibit a significant difference. Furthermore, the error bars in Figure 6 suggest that the uniformity of the dendritic microstructure in the cross-sections improves with increasing distance from the chill plate, implying that grain competition during solidification in the starter block is reduced as the number of grains decreases with increasing distance from the chill plate. Figure 7 presents the microstructure of three cross-sections in the single crystal casting, which have been etched using different etching solutions: Kalling II solution for sections a and b, Marble solution for section c, and V2A solution for section d. In all images, primary dendrites are clearly visible.

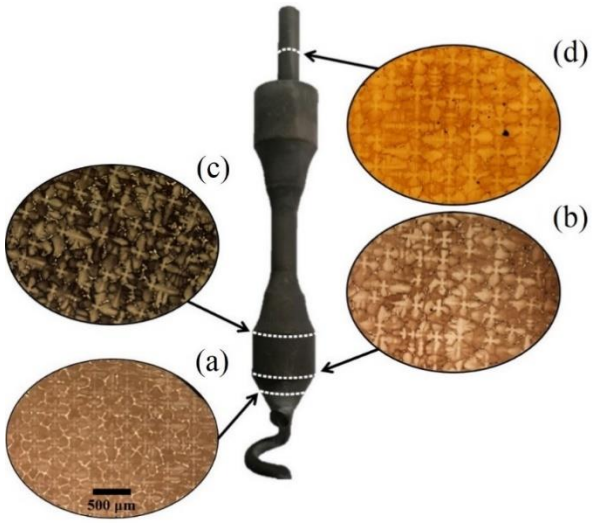

Figure 7. Microstructural images at 50 times magnification of the cross-sections of the single-crystal casting at distances of a)75, b)80, c)95 and d)210 mm from the chill plate.

Based on equation 5 and the primary dendrite counts obtained from the sections in Figure 7, the average distance between primary dendritic arms in sections a, b, c, and d is 281 µm, 336 µm, 336 µm, and 336 µm, with a notable 19.6% increase in λ_1 observed between section a and d. Figure 8 displays the results of calculating λ_1 for the corresponding sections in Figure 7.

The diagram in Figure 8 illustrates the stability of the distance between primary dendrite arms in the single crystal casting. Notably, this distance is dependent on the solidification rate and thermal gradient, as described by equations 1 and 3, respectively. Since the solidification rate is equivalent to the withdrawal rate under stable solidification conditions.

According to Figure 8, the diagram indicates that stable solidification conditions can be achieved at a distance of 80 mm from the chill plate. Furthermore, using equation 3, if λ_1 is taken to be a constant value of 336 µm and the growth rate of the single crystal is equivalent to the withdrawal rate at 0.034 mm/s, the thermal gradient can be calculated as follows:

$$G = \sqrt[0.34]{\frac{255}{\lambda_1 \cdot V^{0.34}}} = \sqrt[0.34]{\frac{255}{336 \times 0.034^{0.34}}} = 13.33 \ \frac{^{\circ}C}{mm}$$

Therefore, it can be concluded that the thermal gradient in the single crystal casting has stabilized after the solidification front reaches a distance of 80 mm from the chill plate, and its value is approximately 13.33°C/mm, as calculated above.

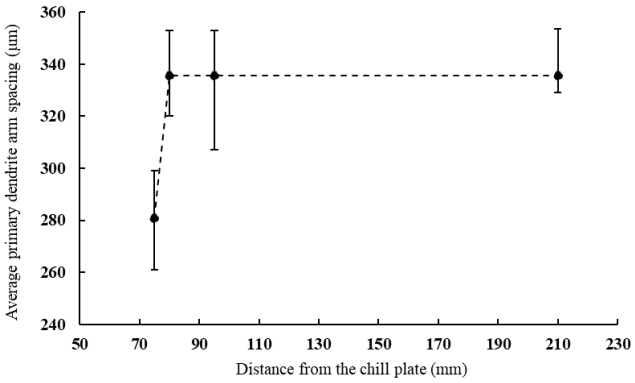

Figure 8. The diagram of the average primary dendrite arm spacing versus the distance from the chill plate in sections a, b, c and d of Figure 7.

Figure 9 presents microstructure images of longitudinal sections at various distances from the chill plate. Notably, secondary dendritic arms are visible in all sections a to d of Figure 9, and the average distance between secondary dendrite arms in these sections is 59 µm, 48 µm, 51 µm, and 57 µm, respectively. The results of calculating the average secondary dendrite arm spacing (λ_2) with error bars are depicted in Figure 10. The presented data reveals that the changes in distance between secondary dendrite arms with increasing distance from the chill plate do not exhibit a discernible trend.

Due to the large dispersion of the results, if section a in Figure 9, which corresponds to the exit section of the grain selector, is excluded, the average secondary dendrite arm spacing has increased by 18.8% from 48 µm to 57 µm in the single crystal area as the distance from the chill plate increases from 69 mm to 200 mm. However, despite the dispersion of results and the overlap of error bars

in Figure 10, there is no statistically significant trend evident.

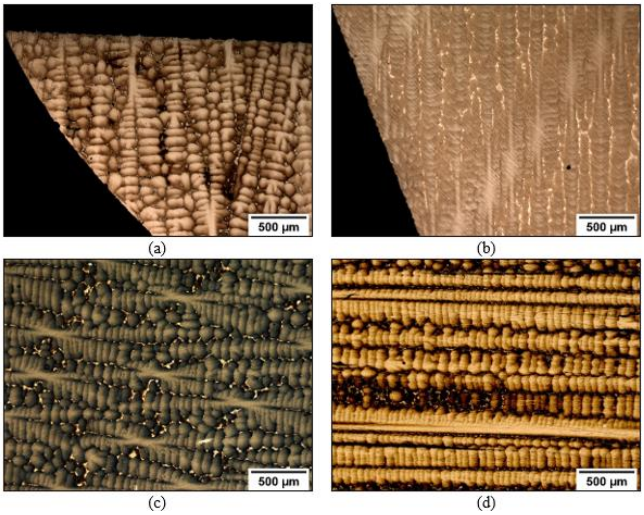

Figure 9. Microstructural images of longitudinal sections at distances a)34, b)69, c)88 and d)200 mm from the chill plate.

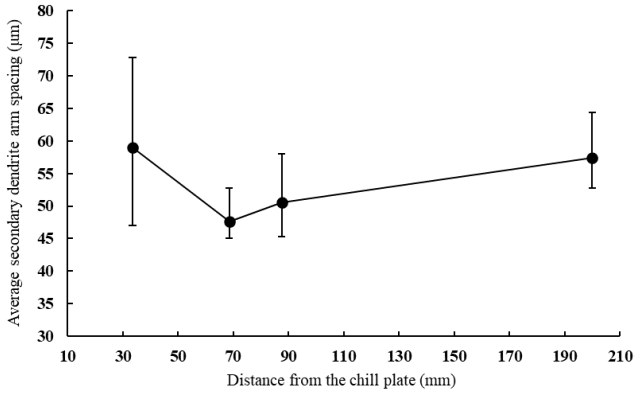

Figure 10. The diagram of the average secondary dendrite arm spacing versus to the distance from the chill plate in sections a, b, c and d of Figure 9.

Rezaei et al. [16] have demonstrated that increasing the distance from the chill plate in a Ni-based superalloy results in a 30% increase in λ_1, as observed in the single-crystal portion of the casting. Matache et al. [9] reported a 15.5% increase in λ_1 and an 18.3% increase in λ_2 as the distance from the chill plate was increased from 85 mm to 235 mm. Matuszewski et al. [17] investigated the correlation between λ_1 and withdrawal rate in CMSX-4, reporting a value of 386 µm at a withdrawal rate of 2 mm/min, which represents a 14.8% increase compared to the present study, despite an associated error bar of 70 µm. Körber et al. [5] also explored the relationship between λ_1 and withdrawal rate, finding a λ_1 value of approximately 320 µm at a withdrawal rate of 2 mm/min, which is remarkably close to the result of this study.

Based on the measured distance between secondary dendrite arms of 57 µm in the single crystal casting, and assuming a solidification rate of 0.034 mm/s, the thermal gradient can be calculated using equation 4 as follows:

$$G = \sqrt[0.35]{\frac{47.83}{\lambda_2 \cdot V^{0.35}}} = \sqrt[0.35]{\frac{47.83}{57 \times 0.034^{0.35}}} = 17.81 \ \frac{^{\circ}C}{mm}$$

Therefore, the thermal gradient calculated using equations 3 and 4 differs by approximately 34%. While the thermal gradient derived from equation 3 appears to be more accurate due to its better stability and lack of dispersion in the results for primary dendrite arm spacing across different cross-sections of the single crystal casting. Additionally, when the thermal gradient calculated using equation 3 is substituted into equation 4, with the solidification rate set equal to the withdrawal rate of 0.034 mm/s, the distance between secondary dendrite arms can be calculated as approximately 63.1 µm, which falls within the range of values presented in Figure 10.

$$\lambda_2 = 47.83(13.33 \times 0.034)^{-0.35} = 63.1 \ \mu m$$

4. Conclusions

The impact of the distance between the solidification front and the chill plate on the microstructural characteristics of CMSX-4 single crystal growth is investigated, and the following results are reported:

1. As the distance from the chill plate increases in the single crystal piece, the primary (λ_1) and secondary (λ_2) dendrite arm spacings increase by 19.6% and 18.8%, respectively.
2. The average primary dendrite arm spacing (λ_1) exhibits a non-uniform increasing trend as a function of distance from the chill plate in the starter block region, with an initially steep slope that gradually decreases. Notably, a 156 µm difference in λ_1 values is observed between the mid-cross-section and the top cross-section of the starter block, corresponding to a 119% increase.
3. In the single crystal region, the changes in the average primary dendrite arm spacing (λ_1) as a function of distance from the chill

plate indicate that a steady state is reached between 80 and 210 mm from the chill plate. The dispersion of the obtained results for λ_1 at distances of 75, 80, 95, and 210 mm from the chill plate is 15%, 10%, 15%, and 8%, respectively.

4. The thermal gradient was calculated to be 13.33 °C/mm based on the average primary dendrite arm spacing (λ_1), assuming equal solidification and withdrawal rates.
5. The average secondary dendrite arm spacing (λ_2) exhibits a 19% increase with increasing distance from the chill plate, from 69 mm to 200 mm. Additionally, the dispersion of the results for λ_2 at distances of 34, 69, 88, and 200 mm from the chill plate is characterized by values of 55%, 17%, 28%, and 27%, respectively.
6. The thermal gradient was calculated to be 17.81 °C/mm based on the average secondary dendrite arm spacing (λ_2), assuming equal solidification and withdrawal rates, which is 34% higher than the value calculated based on the average primary dendrite arm spacing.
7. The stability of the results for the average primary dendrite arm spacing (λ_1) suggests that the thermal gradient calculated using λ_1 is more representative of the real conditions compared to the results obtained for the average secondary dendrite arm spacing (λ_2) due to its better alignment with experimental values.

References

[1] S. Jin, R.S. Ruoff, Preparation and uses of large area single crystal metal foils, APL Mater. 7 (2019). https://doi.org/10.1063/1.5114861.

[2] K. Harris, J.B. Wahl, Improved Single Crystal Superalloys, CMSX-4 (SLS)[La+Y] and CMSX-486, in: Superalloys 2004 (Tenth Int. Symp., TMS, 2004: pp. 45–52. https://doi.org/10.7449/2004/Superalloys_2004_45_52.

[3] A. Basak, S.K. Das, G.W. Woodruff, Effect of Heat Treatment on the Microstructures of CMSX-4 Processed through Scanning Laser Epitaxy (SLE), in: 2017. https://api.semanticscholar.org/CorpusID:210920054.

[4] S. Kostic, A. Golubovic, A. Valcic, Primary and secondary dendrite spacing of Ni-based superalloy single crystals, J. Serbian Chem. Soc. 74 (2009) 61–69. https://doi.org/10.2298/JSC0901061K.

[5] S. Körber, M. Fleck, R. Völkl, U. Glatzel, Anisotropic Growth of the Primary Dendrite Arms in a Single-Crystal Thin-Walled Nickel-Based Superalloy, Adv. Eng. Mater. 24 (2022). https://doi.org/10.1002/adem.202101332.

[6] G. Matache, D.M. Stefanescu, C. Puscasu, E. Alexandrescu, An Investigation of Dendritic Segregation in Directionally Solidified CMSX-4 Superalloy, in: Adv. Sci. Eng. Cast. Solidif., Springer International Publishing, Cham, 2015: pp. 223–230. https://doi.org/10.1007/978-3-319-48117-3_27.

[7] Z. Shen, B. Zhou, Y. Zhong, T. Zheng, W. Ren, Z. Lei, Z. Ren, Revealing influence mechanism of a transverse static magnetic field on the refinement of primary dendrite spacing during directional solidification, J. Cryst. Growth 517 (2019) 54–58. https://doi.org/10.1016/j.jcrysgro.2019.04.010.

[8] P. Auburtin, T. Wang, S.L. Cockcroft, A. Mitchell, Freckle formation and freckle criterion in superalloy castings, Metall. Mater. Trans. B 31 (2000) 801–811. https://doi.org/10.1007/s11663-000-0117-9.

[9] G. Matache, D.M. Stefanescu, C. Puscasu, E. Alexandrescu, Dendritic segregation and arm spacing in directionally solidified CMSX-4 superalloy, Int. J. Cast Met. Res. 29 (2016) 303–316. https://doi.org/10.1080/13640461.2016.1166726.

[10] B. Chmiela, M. Sozańska, Analysis of high angle boundaries in directionally solidified turbine blade made of CMSX-4® superalloy, IOP Conf. Ser. Mater. Sci. Eng. 22 (2011) 012008. https://doi.org/10.1088/1757-899X/22/1/012008.

[11] D. Szeliga, Effect of Processing Parameters and Shape of Blade on the Solidification of Single-Crystal CMSX-4 Ni-Based Superalloy, Metall. Mater. Trans. B 49 (2018) 2550–2570. https://doi.org/10.1007/s11663-018-1347-z.

[12] W. Wan, D. Li, H. Wang, L. Zhao, X. Shen, D. Sun, J. Chen, C. Xiao, Automatic Identification and Quantitative Characterization of Primary Dendrite Microstructure Based on Machine Learning, Crystals 11 (2021) 1060. https://doi.org/10.3390/cryst11091060.

[13] E. Vandersluis, C. Ravindran, Comparison of Measurement Methods for Secondary Dendrite Arm Spacing, Metallogr. Microstruct. Anal. 6 (2017) 89–94. https://doi.org/10.1007/s13632-016-0331-8.

[14] M.F. Moreira, G.P. Souza, B.N. Venturelli, L.B. Fantin, C.R.F. Azevedo, Effect of the Cooling Rate

on the Microstructure of Directionally Solidified Casting (CMSX-4 Ni Superalloy), Int. J. Met. (2024). https://doi.org/10.1007/s40962-023-01249-6.

[15] J.S. Lee, J.H. Gu, H.M. Jung, E.H. Kim, Y.G. Jung, J.H. Lee, Directional Solidification Microstructure Control in CM247LC Superalloy, Mater. Today Proc. 1 (2014) 3–10. https://doi.org/10.1016/j.matpr.2014.09.002.

[16] M. Rezaei, A. Kermanpur, F. Sadeghi, Effects of withdrawal rate and starter block size on crystal orientation of a single crystal Ni-based superalloy, J. Cryst. Growth 485 (2018) 19–27. https://doi.org/10.1016/j.jcrysgro.2017.12.040.

[17] K. Matuszewski, H. Matysiak, J. Jaroszewicz, W. De Nolf, K. Kubiak, K.J. Kurzydłowski, Influence of Bridgman process conditions on microstructure and porosity of single crystal Ni-base superalloy CMSX-4, Int. J. Cast Met. Res. 27 (2014) 329–335. https://doi.org/10.1179/1743133614Y.0000000112.